The Journal of Neuroscience, July 1, 1997, 17(13):5080–5088

Clustering of Voltage-Sensitive Sodium Channels on Axons Is Independent of Direct Schwann Cell Contact in the Dystrophic Mouse

Thomas J. Deerinck,[1] S. Rock Levinson,[2] G. Vann Bennett,[3] and Mark H. Ellisman[1]

[1]National Center for Microscopy and Imaging Research at San Diego and the Department of Neurosciences, University of California San Diego, La Jolla, California 92093-0608, [2]Health Sciences Center, University of Colorado, Denver, Colorado 80262, and [3]Howard Hughes Medical Institute, Duke University Medical Center, Durham, North Carolina 27710

The distribution of voltage-sensitive sodium channels on axons in the dorsal and ventral spinal roots of the dystrophic mouse 129/ReJ–Lama^{2dy} was determined via immunocytochemistry. In these nerves there are regions in which Schwann cells fail to proliferate and myelinate axons in a normal manner, leaving bundles of closely packed large-diameter amyelinated axons. We have identified discrete and focal concentrations of sodium channel immunoreactivity on these axons by both confocal immunofluorescence and immunoelectron microscopy, using a peptide-derived polyclonal antibody. In addition, simultaneous labeling with an antibody recognizing neuronal-specific ankyrin$_G$ revealed a distinct colocalization with the sodium channels on both normal and amyelinated axons. The presence of patches of sodium channels along with their anchoring protein on amyelinated axons in the absence of intervening Schwann cells demonstrates that axons can form and maintain independently these initial aggregations. This confirms that direct contact between Schwann cell and axon is not required for the formation of sodium channel patches of nodal dimensions and density. Furthermore, this strongly suggests that local transfer of sodium channels from Schwann cells to axons is not required for this process.

Key words: sodium channels; ankyrin$_G$; myelination; node of Ranvier; immunocytochemistry; Schwann cell; dystrophic mouse

Myelinated axons produce and maintain focal concentrations of voltage-sensitive sodium channels at fairly regular intervals along their lengths. These concentrations occur most prominently at nodes of Ranvier and are essential for the propagation of action potentials. The processes involved in the myelination of axons by Schwann cells and the development of nodes of Ranvier have been studied extensively by light and electron microscopy. Despite this, controversy remains as to the role that Schwann cells play in inducing the initial aggregation of voltage-sensitive sodium channels on axonal membranes during development and in maintaining these aggregations after myelination. Although some studies in a variety of systems have been interpreted to suggest that the development and maintenance of sodium channel aggregates are dependent on direct Schwann cell involvement (Rosenbluth and Blakemore, 1984; Rosenbluth, 1988; Joe and Angelides, 1992), others suggest that this type of axonal specialization can develop independent of and before glial involvement (Ellisman, 1976; Bray et al., 1979; Ellisman, 1979; Wiley-Livingston and Ellisman, 1980; Smith et al., 1982; Waxman et al., 1982).

Efforts to chronicle the synthesis and aggregation of sodium channels on the developing axons of neonatal mice and rats *in vivo* have been met with difficulties primarily because of limitations in detection sensitivity, the complexity of the developing environment, and the rapid and asynchronous manner in which myelination occurs. Studies of developing rat sciatic nerve have revealed a close association of adherent Schwann cell processes to sodium channel cluster formation on axons (Vabnick et al., 1996). However, in this recent work it could not be determined whether contact by Schwann cell processes induced clustering on axons or instead whether the processes simply were attracted chemotactically to preexisting sites.

Dystrophic mice of the strain 129/ReJ–Lama^{2dy} have a genetic defect in the expression of merosin (laminin α 2) that leads, among other things, to a defect in the formation of a normal basement membrane (Sunada et al., 1994; Xu et al., 1994). Merosin has been implicated in both Schwann cell mitogenesis and migration (Engvall et al., 1992; Anton et al., 1994). This merosin deficiency results in abnormal Schwann cell–axon interactions characterized by short internodal lengths, thin myelin sheaths, heminodes of Ranvier, and, more importantly for the present work, large regions containing bundles of closely packed naked axons in the dorsal and ventral spinal roots of these mice that are completely devoid of Schwann cells (Bradley and Jenkison, 1973; Stirling, 1975). These unensheathed and amyelinated axons have diameters of ~2–6 μ and may remain unmyelinated for as much as 10–15 mm (Bradley and Jenkison, 1973). The spinal roots of these mutant mice have been studied extensively, and the ultrastructure provides no evidence for Schwann cell degeneration but, rather, indicates that these regions of amyelinated axons are probably the result of an inability of Schwann cells to proliferate and migrate in a normal manner (Bray and Aguayo, 1975; Stirling, 1975). This model system provides a unique opportunity to study the respective roles of axon and Schwann cell in the formation and maintenance of sodium channel aggregations.

Received Dec. 2, 1996; revised April 17, 1997; accepted April 23, 1997.

This study was supported by National Institutes of Health Grants NS15879 to S.R.L. and RR04050, NS14718, and NS26739 to M.H.E.

Correspondence should be addressed to Dr. Mark H. Ellisman, National Center for Microscopy and Imaging Research, Department of Neurosciences, University of California San Diego, School of Medicine, Basic Sciences Building, Room 3032, 9500 Gilman Drive, La Jolla, CA 92093-0608.

MATERIALS AND METHODS

Antibody production and characterization. An 18-mer peptide (TEEQKKYYNAMKKLGSKK), designated EOIII and representing a highly conserved portion of the domain III–IV linker of vertebrate sodium channels, was synthesized with a C-terminal cysteine to allow for maleimide coupling to carrier protein and affinity gels. This peptide was purified by reverse-phase HPLC, conjugated to Keyhole Limpet hemocyanin with the Imject kit (Pierce, Rockford, IL), and used to immunize rabbits at 4 week intervals. One of the resulting antisera, designated 1380, exhibited high titers to purified eel electroplax Na^+ channels. This antiserum was affinity-purified on an EOIII-coupled column (Immuno-Pure Ag/Ab Immobilization Kit 2, Pierce). Further details of purification and characterization are given in Dugandzija-Novakovic et al. (1995). Rabbit (Kordeli et al., 1995) and chicken (Zhang and Bennett, 1996) antibodies against 480 and 270 kDa isoforms of ankyrin$_G$ were affinity-purified and characterized as described previously. Briefly, antibodies against the common tail region of rat ankyrin$_G$ 480 and 270 kDa were raised in chickens (residues 1821–2337) or rabbits (residues 1613–1950) immunized with purified recombinant polypeptides. Recombinant polypeptides were expressed in bacteria as fusion proteins with the viral gene 10 polypeptide by using the pGemex expression vector. Chicken antibodies were isolated from chicken egg yolk by an Egg Yolk Purification Kit (Pharmacia Biotech, Piscataway, NJ) and affinity-purified against purified recombinant polypeptide immobilized on Sepharose CL-6B (Pharmacia) after the previous depletion of antibodies against the gene 10 protein. Rabbit antibodies were affinity-purified from antisera after depletion of gene 10 immunoreactivity.

Preparation of tissue for electron microscopy and immunocytochemistry. Dystrophic mice (4- to 6-week-old) of the strain 129/ReJ–Lama^{2dy} (Jackson Laboratories, Bar Harbor, ME) and their control heterozygous littermates were anesthetized with 4 ml/kg of body weight ketamine/Rompun and perfused by intracardiac catheterization. Perfusion with a balanced salt solution containing (in mM): 135 NaCl, 14 $NaHCO_3$, 1.2 Na_2HPO_4, 5 KCl, 2 $CaCl_2$, and 1 $MgCl_2$ at 35°C was followed by 4% formaldehyde (fresh from paraformaldehyde) in 0.1 M PBS pH 7.4 for 5 min. Dorsal and ventral spinal roots were removed carefully and fixed for an additional 1 hr, after which they were rinsed in PBS and incubated in 1 mg/ml collagenase (Sigma, St. Louis, MO) in PBS for 20 min at room temperature. Individual roots were teased under high-power stereoscopic observation into bundles consisting of several dozen axons and rinsed with PBS.

Confocal microscopy. Fixed and teased nerves were permeabilized in a solution containing 0.2% Triton X-100, 1% normal goat serum, and 1% cold-water fish gelatin (Sigma) in PBS for 30 min before incubation in affinity-purified anti-sodium channel antibody (AP1380) for 18 hr at 4°C, washed in buffer, and incubated in donkey anti-rabbit IgG-FITC conjugate (Jackson ImmunoResearch, West Grove, PA) in PBS containing 5 μg/ml propidium iodide for 1 hr at 4°C. After this, the nerves were rinsed in PBS and mounted in Gelvatol. For colabeling with ankyrin$_G$, nerves were incubated in the antibody AP1380 simultaneously with a chicken-derived anti-ankyrin$_G$ antibody for 18 hr at 4°C, washed in buffer, and incubated in donkey anti-rabbit IgG-FITC and donkey anti-chicken IgY–CY5 conjugates that had been preabsorbed for species specificity (Jackson ImmunoResearch) and diluted in PBS containing 5 μg/ml propidium iodide for 1 hr at 4°C. After this the nerves were rinsed in PBS and mounted in Gelvatol. Confocal microscopy was performed with an MRC-1024 system (Bio-Rad, Hercules, CA) attached to an Axiovert 35M microscope (Zeiss AG, Oberkochen, Germany) with a 40× 1.3 numerical aperture objective. Excitation illumination was with 488, 568, and 647 nm light from a krypton/argon laser. Individual images (1024 × 1024 pixels) and z-series stacks (10–20 images at 0.5 μ z-spacing) were saved to optical disk (Pinnacle Micro), converted to PICT format, and merged as pseudocolor images with Adobe Photoshop (Adobe Systems, Mountainview, CA). Because of the overlap of sodium channel and ankyrin$_G$ immunoreactivity, the triple-labeled images were displayed as two dual-fluorescence images side by side for clarity. Digital prints were from a Fujix Pictrography 3000 printer (Fuji, Tokyo, Japan).

Immunoelectron microscopy. Fixed, teased, and permeabilized nerves were incubated in either AP1380 or a rabbit anti-ankyrin$_G$ antibody for 18 hr, washed in buffer, and incubated in biotinylated goat anti-rabbit IgG for 1 hr at 4°C. After washes in PBS, the nerves were incubated in an avidin–biotin complex (Vector Laboratories, Burlingame, CA) for 1 hr, washed again in PBS, and reacted for 6 min in 0.05 mg/ml diaminobenzidine tetrahydrochloride (Sigma) with 0.01% H_2O_2. Then the nerves were post-fixed with 1% OsO_4 in PBS for 1 hr, rinsed in DDH_2O, dehydrated in an ethanol series, and embedded in Durcupan resin (Electron Microscopy Sciences, Fort Washington, PA). For conventional electron microscopy, mice were perfused with 2% glutaraldehyde and 2% formaldehyde in 0.15 M sodium cacodylate, post-fixed with 2% OsO_4, and dehydrated and embedded as described above. Thin (100 nm) sections and semithin (1–2 μ) sections were cut with a diamond knife (Diatome, Fort Washington, PA) and an Ultracut E ultramicrotome (Leica, Nusslock, Germany) and mounted on uncoated copper grids. Thin sections were imaged at 80 kiloelectron volts (keV) with a 100CX or 2000FX electron microscope (JEOL, Tokyo, Japan), and semithin sections were imaged at 300–400 keV with a 4000EX intermediate-voltage electron microscope (JEOL). Stereopair electron micrographs were obtained by tilting the specimen ±5°. For measuring patch distribution, large (2 × 3 mm) 100-nm-thick sections were mounted on slot grids, and multiple adjacent images were recorded at 2000× magnification. The resultant negatives were digitized and montaged together by Adobe Photoshop. Outlines of individual axons were traced, and immunoreactive patches were identified.

RESULTS

Confocal microscopy

The dorsal and ventral spinal roots from formaldehyde-fixed 4-to 6-week-old dystrophic mice and their otherwise normal heterozygous littermates were prepared for immunolocalization of sodium channels and neuronal-specific ankyrin$_G$ by laser scanning confocal microscopy. To visualize the distribution of Schwann cells and other non-neuronal cell types, we costained teased nerve bundles with propidium iodide to reveal the distribution of RNA and DNA. Observations of teased fibers from normal littermates revealed focal concentrations of sodium channel immunoreactivity corresponding to nodes of Ranvier (Fig. 1*A*). Many Schwann cells could be seen throughout the diameter of the nerve bundles, and no sodium channel immunoreactivity was observed on Schwann cell membranes. In addition to sodium channels, nerves also were immunolabeled simultaneously for neuronal-specific ankyrin$_G$. Ankyrin$_G$ is a component of the distinctive dense plaque of material on the cytoplasmic surface of the nodal axonal membrane (Kordeli et al., 1990, 1995), and it is a specialized isoform of a family of spectrin-binding proteins that associate via their membrane-binding domains with diverse integral proteins (Bennett and Gilligan, 1993). Ankyrin$_G$ is a candidate for participation in a complex involving the voltage-sensitive sodium channel and the spectrin/actin network at nodes of Ranvier, based on observations that the voltage-dependent sodium channel copurifies from brain and associates *in vitro* with ankyrin (Srinivasan et al., 1988). As can be seen in Figure 1*B*, the distribution of ankyrin$_G$ correlated closely to the distribution of sodium channels.

Teased fiber bundles from the dystrophic mice contained large regions of closely packed amyelinated axons, many of which were devoid of intervening cells. These regions could be distinguished by the absence of propidium iodide staining in nerve bundles. In these regions of amyelinated axons numerous discrete and intense patches of sodium channel immunoreactivity were observed (Fig. 1*C*). The staining appeared most often as asymmetrical patches and, to a lesser extent, as rings around the axons. In many instances the dimensions of these patches appeared to be somewhat more extended in the longitudinal axis of the axon, as compared with those found at normal nodes of Ranvier. Cells stained by propidium iodide and representing, for the most part, Schwann cells can be seen at the periphery of the fiber bundles. Colabeling for ankyrin$_G$ immunoreactivity revealed a close association with these sodium channel clusters (Fig. 1*D*).

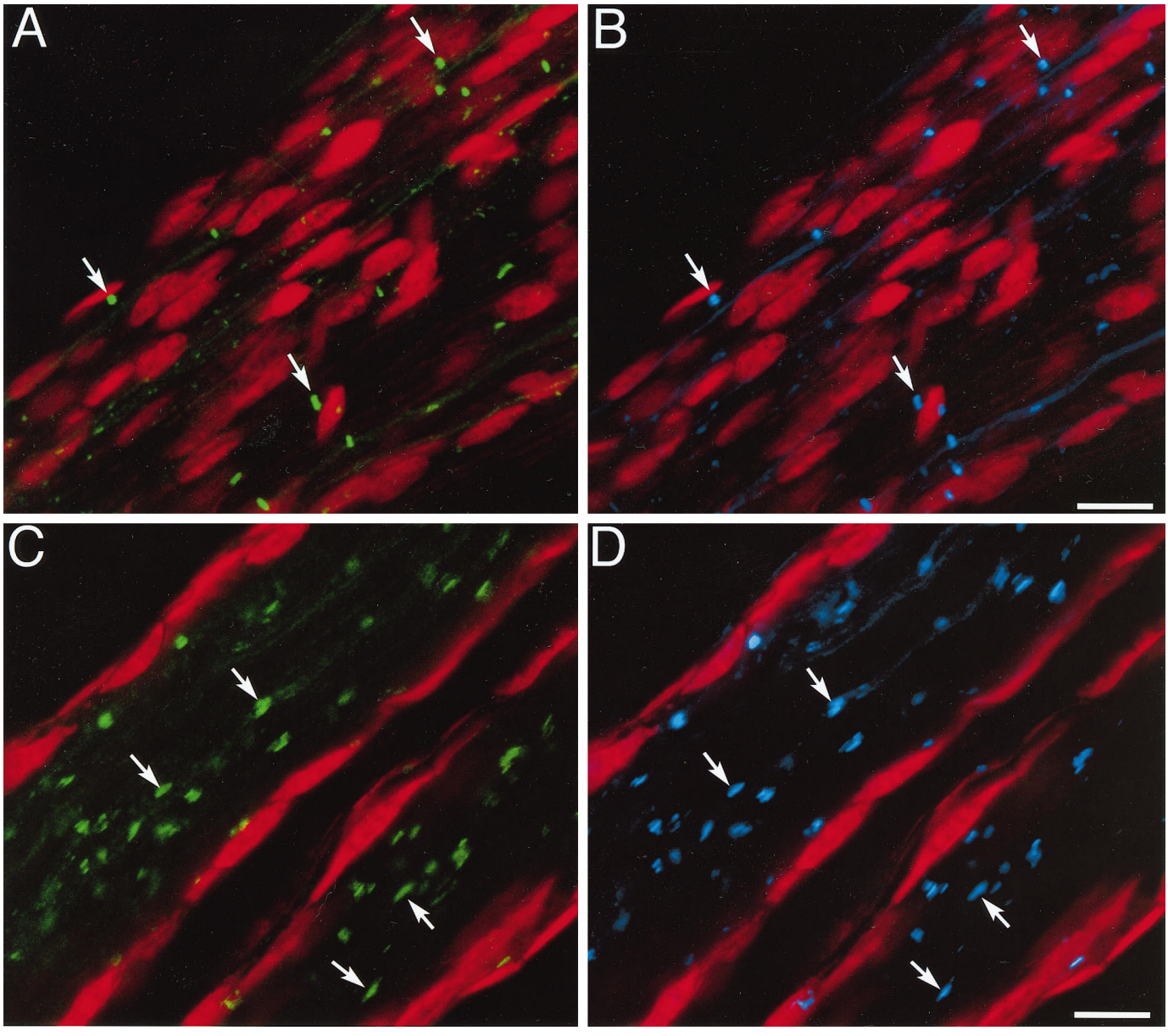

Figure 1. Confocal immunofluorescent images of the distribution of sodium channel and ankyrin$_G$ immunoreactivity in normal and dystrophic spinal roots. Images were taken from the midpoint of the fiber bundle diameter, as determined by optical sectioning. *A*, A single teased fiber bundle from a 5-week-old normal mouse immunolabeled for sodium channels (*green*) and stained with propidium iodide (*red*) revealed intense sodium channel immunoreactivity at discrete sites corresponding to nodes of Ranvier (*arrows*). Schwann cells stained by propidium iodide can be seen throughout the diameter of the fiber bundle. *B*, The same fiber bundle was immunolabeled simultaneously for ankyrin$_G$ (*blue*), which showed a close colocalization with sodium channel immunoreactivity. *C*, Shown are two adjacent teased fiber bundles from a 5-week-old dystrophic mouse immunolabeled for sodium channels (*green*) and stained with propidium iodide (*red*). Clusters of sodium channels are found throughout the diameter of the bundle, most notably in the central portion, which contains many large amyelinated axons (*arrows*). Schwann cells stained by propidium iodide can be seen on the periphery of the fiber bundle. *D*, The same fiber bundles were immunolabeled simultaneously for ankyrin$_G$ (*blue*) and showed a colocalization with sodium channel immunoreactivity. Scale bars, 10 μm.

Immunoelectron microscopy

Observations by electron microscopy of glutaraldehyde-fixed spinal roots from the dystrophic mouse revealed differing regions of Schwann cell–axon interactions. Although some areas consisted of apparently normally myelinated axons, nodes of Ranvier, and partially myelinated axons that formed heminodes, others contained regions of large-diameter (2–6 μ) amyelinated axons without any intervening Schwann cells (Fig. 2). The prevalence of these large-diameter closely packed amyelinated axons increased in the sacrolumbar roots at midlength and could be identified easily by the translucent appearance of the nerve rootlet by light microscopy. These regions were selected for immunoelectron microscopy.

Because the epitope recognized by the anti-sodium channel antibody (AP1380) is on an intracellular domain, immunolocalization of this protein required the prepermeabilization of the axons with a minimum of 0.2% Triton X-100. Furthermore, this epitope contains a lysine-rich domain, which obviated the use of even low concentrations of glutaraldehyde. For these reasons the preservation of axonal membranes was compromised somewhat.

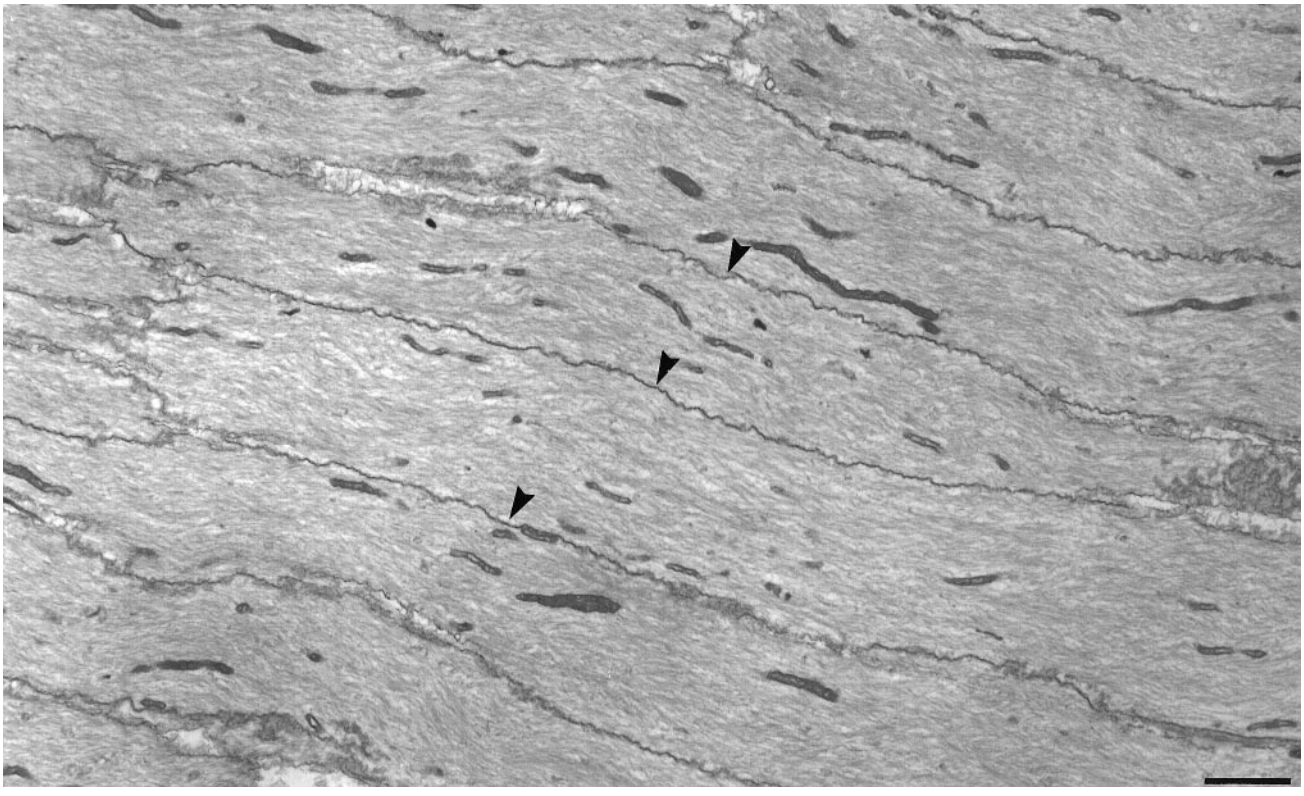

Figure 2. Electron micrograph of a conventionally fixed spinal root from the dystrophic mouse. Many large-diameter (>2 μm) amyelinated axons lie in very close proximity to each other (*arrows*) without intervening cells. These axons occur more frequently in the central portion of the fiber bundles at midlength, and we observed them to remain Schwann cell-free for at least several hundreds of microns in length. Scale bar, 2 μm.

In thin sections immunostained preparations of amyelinated axons revealed numerous distinct focal patches of sodium channel immunoreactivity along the axolemma (Fig. 3*A*). The shape of this immunoreactivity most often resembled an asymmetrical patch on one side of the axon, although a significant number of axons also exhibited symmetrical staining around their diameters as a torus. The edge of these patches showed a sharp delineation (Fig. 3*B*) and usually ranged in size from ~1–2 μ in their longitudinal axis (Table 1). No constriction of the axon diameter was observed in the regions of staining, and no staining of the axolemma between patches was observed. Also, it generally was observed that patches occurred on adjacent axons with a greater frequency than what would be expected if they were distributed randomly. In regions containing heminodes of Ranvier, immunoreactivity was observed on the axolemma immediately adjacent to the paranodal region. The staining pattern was usually symmetrical around the axon, but asymmetrical staining also was observed (Fig. 3*C*). Immunolocalization of ankyrin$_G$ on amyelinated axons revealed patches of immunoreactivity that were very similar in size and shape to those found with sodium channels (Fig. 3*D*). Ankyrin$_G$ immunoreactivity also was observed at heminodes of Ranvier (data not shown). In normal control preparations sodium channel and ankyrin$_G$ immunoreactivity was observed only at nodes of Ranvier. In regions of spinal roots from this mutant that contained apparently normally myelinated axons, sodium channel and ankyrin$_G$ immunoreactivity was identical to that found at normal nodes of Ranvier.

To determine whether these regions of amyelinated axons were completely devoid of Schwann cell processes and to visualize better the three-dimensional shape of sodium channel immunoreactivity, serial thick sections were imaged by using intermediate-voltage electron microscopy (300–400 keV). Observations of stereopair images of 1-μ-thick sections again revealed very discrete regions of sodium channel immunoreactivity in regions without any intervening cell processes (Fig. 4*A*). Discrete sodium channel immunoreactivity often was observed on axons in which no Schwann cells were visible within at least 100 μ of their length and within >10 μ laterally. At higher magnification the discrete shape and uniformity of sodium channel immunoreactivity on the axon could be appreciated (Fig. 4*B*). In general, although the shape of individual patches was diverse, their overall size fell within a fairly narrow range. Measurement of the average surface area of individual patches on axons was not made.

The close packing of the amyelinated axons made it impossible to determine the average distance between patches on individual axons by confocal microscopy. Furthermore, if the fiber bundles were teased further into individual axons, one could not be certain that the axons being studied had not developed immediately adjacent to Schwann cells. To determine whether there was a regular interpatch spacing along amyelinated axons, we created a low-magnification montage of 12 thin-section electron micrographs covering an area ~35 μ wide and 400 μ long (Fig. 5). Axon diameter, length, and interpatch distance data are given in Table 1. In this montage we were able to follow 25 individual axons for distances >35 μ and seven axons for >100 μ, with a total number of 35 patches identified. Of these 35 patches, nine showed symmetrical staining on each side of the axon. On 20 of the axons we found only one visible patch, in which case we measured the distance from the edge of the patch to the furthest point on the axon visible in the montage. On the five axons for which we could

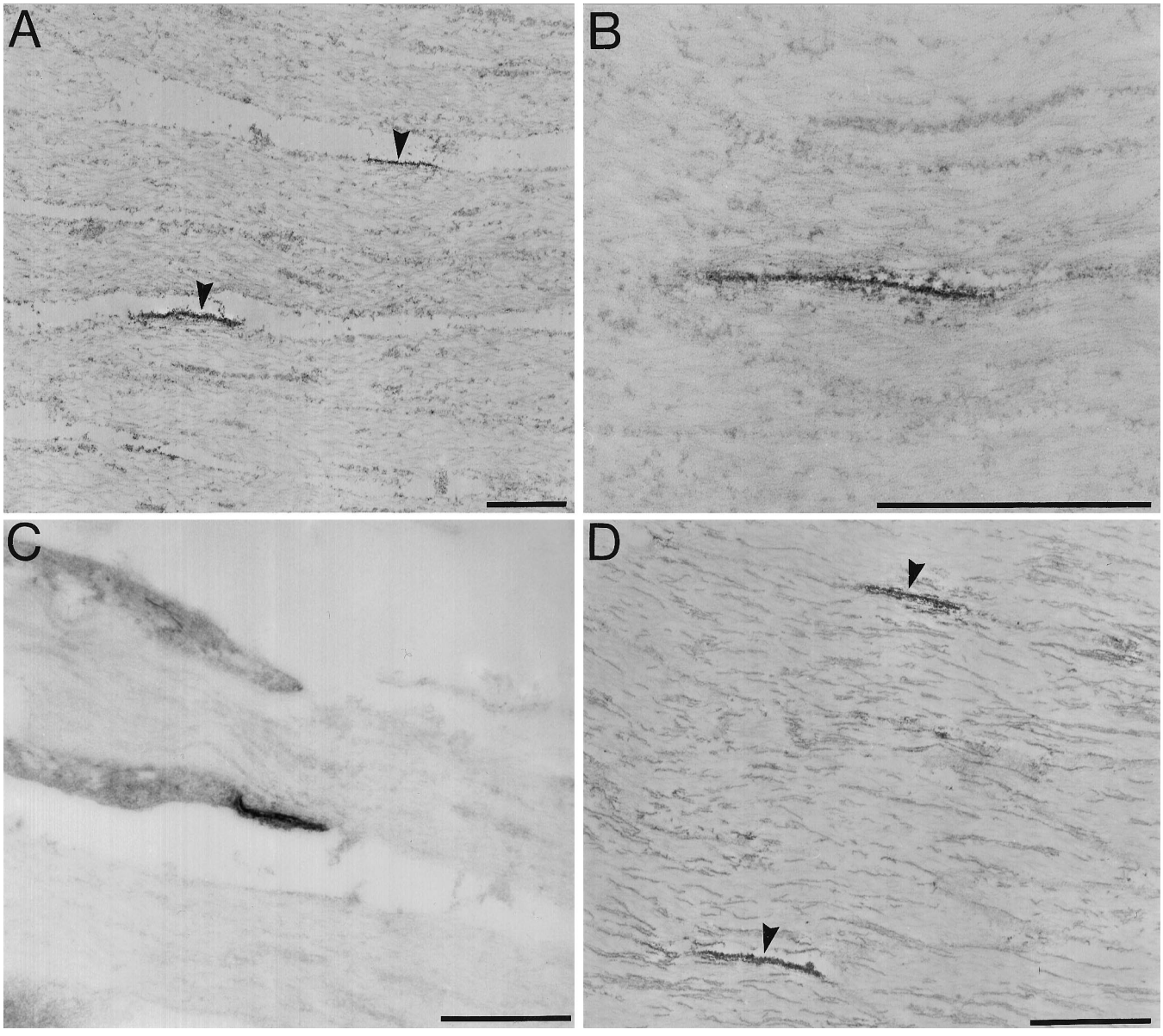

Figure 3. Immunolocalization of sodium channels and ankyrin$_G$ by electron microscopy on axons from the dystrophic mouse. *A*, Two separate clusters of sodium channel immunoreactivity can be seen on adjacent axons in a region consisting exclusively of amyelinated axons (*arrows*). *B*, At higher magnification the sharp delineation of the edges of a typical sodium channel immunoreactive patch can be seen. *C*, Sodium channel immunoreactivity was observed on the axolemma at heminodes of Ranvier. In some instances the immunoreactivity had an asymmetrical distribution on the axonal membrane. *D*, Ankyrin$_G$ immunoreactivity appeared very similar to that observed for sodium channels. Scale bars, 2.5 μm.

identify more than one patch, the distance between patches ranged from 16 to 125 μ and averaged 61.2 μ. In general it was observed that multiple patches rarely occurred within 25 μ of each other on an individual axon.

DISCUSSION

Of central importance in understanding the basic mechanisms involved in myelination and remyelination is the elucidation of the respective roles that axons and Schwann cells play in the induction of ion channel aggregation that occurs early in development. The merosin-deficient dystrophic mouse model is unique in that there are large regions in the spinal roots with greatly reduced numbers of Schwann cells that, for the most part, remain peripheral to axon bundles, giving rise to large-diameter closely packed amyelinated axons that develop and remain Schwann cell-free for hundreds of microns along their length. In the present study we demonstrate that these axons can form and maintain aggregates of voltage-sensitive sodium channels on their surfaces without direct Schwann cell contact. This model system has been used previously to identify by freeze fracture clusters of node-like intramembranous particles at heminodes of Ranvier and on the axolemma of these closely packed amyelinated axons (Ellisman, 1976, 1979; Bray et al., 1979; Wiley-Livingston and Ellisman, 1981).

In addition to sodium channels, Na^+–K^+ ATPase also has been shown to reside in high concentrations at normal nodes of Ranvier (Wood et al., 1977; Ariyasu et al., 1985). However, in marked contrast to normal peripheral nerve, isoforms of Na^+–K^+ ATPase on amyelinated axons of the dystrophic mouse have a

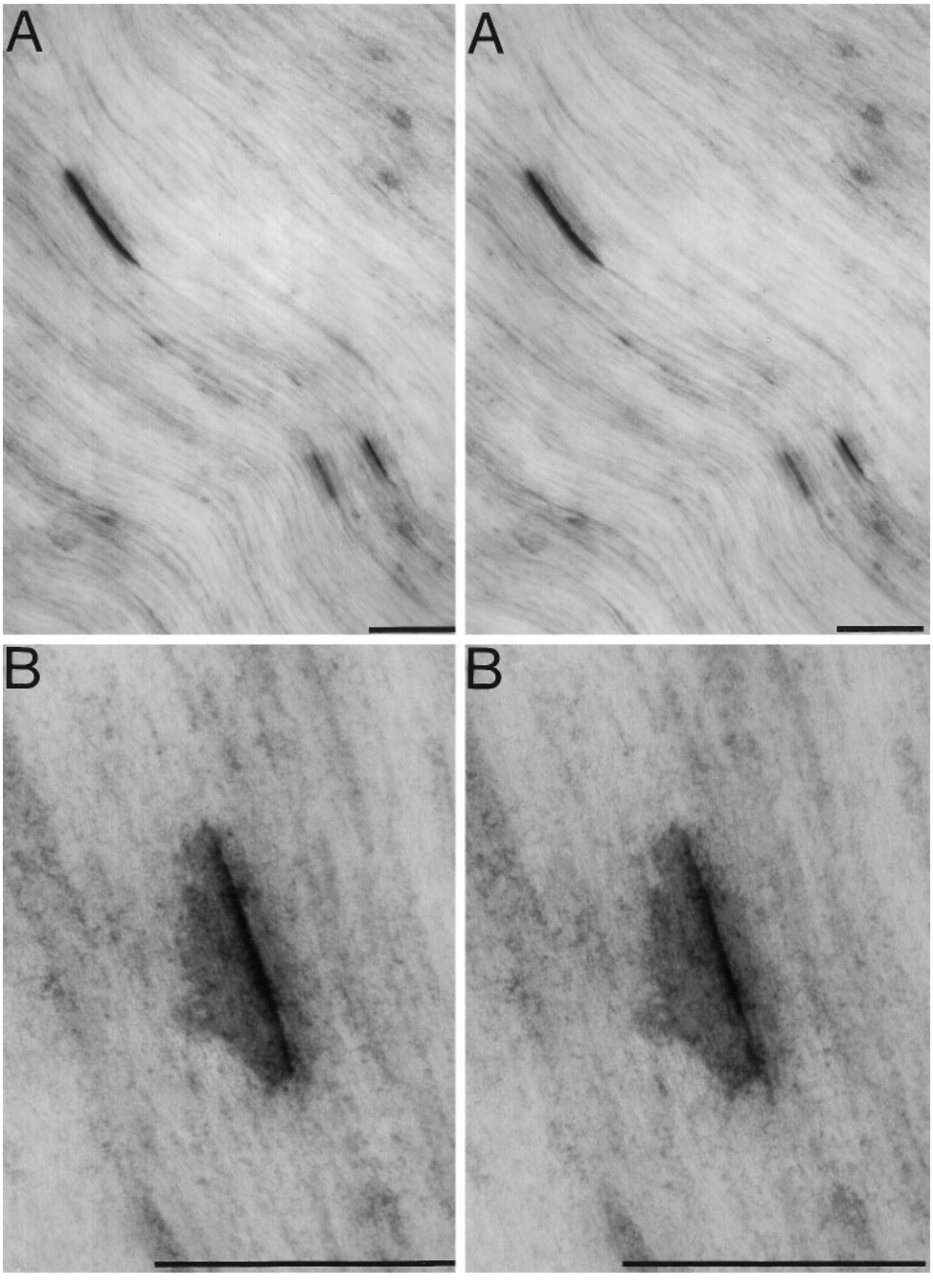

Figure 4. Thick-section stereopair electron micrographs of sodium channel immunoreactivity on amyelinated axons of the dystrophic mouse. *A*, Low-power image showing asymmetrical and symmetrical sodium channel immunoreactivity on axons. *B*, Higher power image of an individual cluster of sodium channel immunoreactivity. Scale bars, 2.5 μm.

continuous distribution along the axolemma (Ariyasu and Ellisman, 1987), indicating that the intramembranous particles observed at heminodes and on amyelinated axons do not represent focal accumulations of the Na^+–K^+ ATPase. However, the present data seem to confirm that the particle aggregates observed by freeze fracture indeed included sodium channels, as previously suggested.

Studies of normal developing peripheral and optic nerve by freeze fracture have demonstrated that there are axonal membrane specializations that precede elaboration and myelination by Schwann cells and oligodendrocytes (Wiley-Livingston and Ellisman, 1980; Waxman et al., 1982). However, attempts to correlate the earliest appearance of sodium channels and their subsequent clustering in normal developing axons by immunocytochemistry have been hampered by limitations in the sensitivity of currently available antigen–antibody detection systems.

In normal myelinated nerve, nodes of Ranvier (and thus sodium channel immunoreactivity) occur at fairly regular intervals along axons at a frequency of ~100 times the axon diameter (Friede and Beuche, 1985). Of great interest is whether the distribution frequency of sodium channel patches on amyelinated axons shows a similar correlation. Although generally it was observed that patches rarely occurred within 25 μ of each other and averaged ~60 μ between patches on individual axons, this type of analysis was difficult for a number of reasons. The close packing of amyelinated axons precluded the use of light microscopy, and the task of following significant numbers of individual axons for hundreds of microns along their lengths in thin sections by elec-

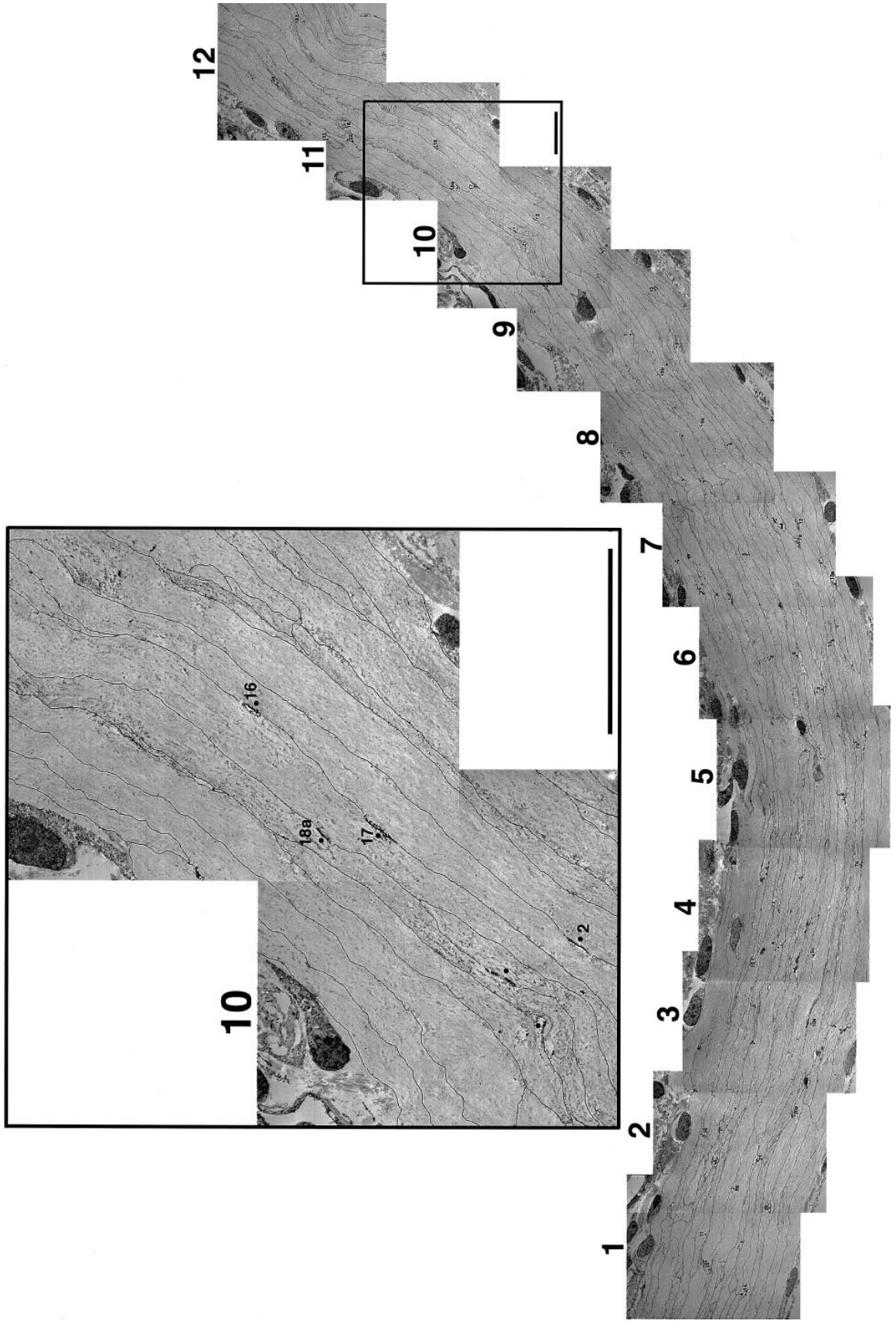

Figure 5. To estimate sodium channel patch frequency, we made a montage of 12 thin-section electron micrographs of dystrophic mouse nerve stained for sodium channels. Images were digitized and montaged, the axon perimeters were traced, and individual patches were located and numbered. The area represents a field of ~35 × 400 μm. The *boxed area* is shown at higher magnification. Scale bars, 10 μm.

Table 1. The distribution of sodium channel immunoreactivity on amyelinated axons

Axon number	Axon diameter (μ)	Axon length (μ)	Number of patches	Patch size (μ)	Distance between patches (μ)	Minimum distance w/o adjacent patch (μ)
1	4.0	37.5	1A	1.0		17.5, 20.0
2	4.0	110.25	1A	1.6		91.0, 21.5
3	2.25	50.0	1A	1.5		17.5, 32.5
4	2.25	50.0	1A	1.0		37.5, 12.5
5	3.6	208.5	3A 1S	1.5, 0.6, 1.2, 0.9	125.0, 70.0, 16.0	
6	2.0	68.5	1A	0.9		43.5, 25.0
7	4.0	187.5	3A 1S	1.3, 1.0, 1.4, 1.3	55.0, 50.0, 27.5	
8	4.0	162.5	1A 1S	0.9, 2.3	95.0	
9	2.0	42.5	1A	1.5		25.0, 17.5
10	3.5	127.5	2A	0.7, 2.1	90.0	
11	2.0	36.0	1A	1.1		25.0, 11.0
12	3.5	69.0	1A	2.1		60.0, 9.0
13	3.5	125.0	1A 1S	1.9, 1.1	81.5	
14	2.0	37.5	1S	1.4		37.5
15	3.5	62.5	1A	1.3		35.0, 27.5
16	3.5	67.5	1A	1.3		44.0, 22.5
17	4.0	102.5	1A	2.4		67.5, 35.0
18	3.5	92.5	1A 1S	1.2, 0.9	31.0	
19	4.0	50.0	1A	1.2		40.0, 10.0
20	4.0	58.5	1A	2.0		35.0, 23.5
21	3.0	52.5	1A	0.7		30.0, 22.5
22	3.0	92.5	1A	2.1		52.5, 40.0
23	3.0	37.5	1S	1.8		30.0, 7.5
24	3.5	43.5	1S	1.2		43.5
25	3.5	57.5	1S	1.2		45.0, 12.5

Measurement data from the montage. The 25 axons that could be followed for at least 35 μ were measured for maximum observed axon diameter, individual axon length, number of visible sodium channel patches per axon and their shape, size of individual patches, and distance between multiple patches on individual axons. On axons in which only one patch was visible, the distance from the edge of the patch to the furthest point on the axon that was visible in the montage was measured. All measurements are in microns (μ). In column 4, patches were identified as being either asymmetrical (A) or symmetrical (S) in appearance.

tron microscopy is technically formidable. This greatly limited the number of measurements that could be made. Nonetheless, an estimation of the frequency distribution of sodium channel immunoreactive patches could be inferred from the number of patches observed as a function of total axonal length measured. Because we observed 35 patches on a total axonal length of 2035 μ, on average there was one detectable patch for every 58 μ of axon. Results from this method of estimation are in general agreement with the directly measured interpatch distance of ~60 μ for the 10 instances we observed. Thus, preliminary measurements indicate that the patch frequency on amyelinated axons from dystrophic mice appears to be shorter than the internodal distances found in the same fibers in normally myelinated mice. However, it is not unreasonable to expect that these patches of sodium channels would be subject to gradual lateral migration over a period of time after their formation in the absence of Schwann cell contact.

Mechanisms of cluster induction and anchoring

The existence of focal sodium channel immunoreactivity on amyelinated axons clearly demonstrates that direct and local Schwann cell contact is not required to produce and maintain discrete concentrations of these channels and augers for an equivalent mechanism to be operant in normal developing nerve. Furthermore, these results strongly contradict the hypothesis that transcytosis of sodium channels from Schwann cell to axon is responsible for sodium channel cluster formation in normal nerve (Ritchie et al., 1990). Although our data denigrate aspects of this hypothesis pertaining to initial sources of sodium channels, these data do not exclude the possibility that Schwann cell sodium channels are contributed to axons in mature nerve. However, to our knowledge there are no data that directly support the transcytosis hypothesis. In previous studies involving demyelination by lysolecithin, clusters of sodium channels often were observed just beyond the tips of adherent remyelinating Schwann cell processes, and these clusters appeared to fuse as Schwann cells approached each other during nodal reformation (Dugandzija-Novakovic et al., 1996). This observation suggested an ability for Schwann cells to somehow organize and move clusters along axons, possibly in part by forming a barrier to channel diffusion. However, our data demonstrate that axons can form aggregates of sodium channels *in vivo* without the direct contact of Schwann cells. Similar inferences were made in a study of chemically treated peripheral axons in fish that were chronically demyelinated (England et al., 1990). In the present study we also show that ankyrin$_G$ colocalizes with sodium channel immunoreactivity on bare axons. Thus, it does not seem necessary to invoke a Schwann cell-dependent diffusional barrier in sodium channel cluster formation. Furthermore, Schwann cell contact is clearly not essential to the organization of cytoskeletal elements thought to anchor sodium channels. Instead, the close association of Schwann cell processes to sodium channel clusters observed in remyelinating systems may be a result of their chemotactic affinity for and rapid migration to preexisting sites of cluster formation.

How then might previous observations suggesting Schwann

cell-dependent cluster formation be reconciled with the present results? One possible explanation is that both phenomena may, in part, reflect the action of a diffusible factor that is released by Schwann cells and initiates sodium channel aggregation by the axon. If the release of such a substance by Schwann cells were relatively low, then cluster formation would be most rapid when Schwann cells were very close or in direct contact with the axon (e.g., during the initial stages of myelination). In the previous work cited above, such clusters were seen very soon after the Schwann cell first contacts the axon and before the formation of compact myelin. However, in the absence of direct contact with Schwann cells, low levels of a diffusible signal released from Schwann cells at more remote locations still might induce more slowly the formation of clusters on the bare axons.

For acetylcholine receptors on muscle, a diffusible clustering factor has been identified as agrin, which is released by the innervating presynaptic terminal during synapse formation (Nitkin et al., 1983). More recently, agrin has been reported to induce sodium channel clustering on cultured muscle fibers (Sharp and Caldwell, 1996). For myelinated nerve fibers, evidence of the existence of such a soluble and diffusible cluster-inducing factor recently has been demonstrated in a CNS model. Work from the laboratory of Barbara Barres on the distribution of sodium channels on cultured rat retinal ganglion cells has shown that the addition of an oligodendrocyte-conditioned cell-free medium can initiate sodium channel aggregation rapidly along these cells (Kaplan et al., 1996). Most strikingly, these aggregations occurred at regularly spaced intervals along the axons at a frequency in direct correlation with the axonal caliber without any glial–axonal contact. The soluble signaling agent involved in this CNS model has yet to be characterized. Taken together with the present results, current knowledge suggests that, whereas Schwann cells may signal for the initiation of sodium channel clustering and formation of nodes of Ranvier, it is the axon that accomplishes the aggregation and determines the initial sites of node formation.

REFERENCES

Anton ES, Sandrock AW, Matthew WD (1994) Merosin promotes neurite growth and Schwann cell migration *in vitro* and nerve regeneration *in vivo*: evidence using an antibody to merosin, ARM-1. Dev Biol 164:133–146.

Ariyasu RG, Ellisman MH (1987) The distribution of ($Na^+ + K^+$) ATPase is continuous along the axolemma of unensheathed axons from spinal roots of "dystrophic" mice. J Neurocytol 16:239–248.

Ariyasu RG, Nichol JA, Ellisman MH (1985) Localization of sodium/potassium adenosine triphosphate in multiple cell types of the murine nervous system with antibodies raised against the enzyme from kidney. J Neurosci 5:2581–2596.

Bennett V, Gilligan DM (1993) The spectrin-based membrane skeleton and micron-scale organization of the plasma membrane. Annu Rev Cell Biol 9:27–66.

Bradley WG, Jenkison M (1973) Abnormalities of peripheral nerves in murine muscular dystrophy. J Neurol Sci 18:227–247.

Bray GM, Aguayo AJ (1975) Quantitative ultrastructural studies of the axon–Schwann cell abnormalities in the spinal nerve roots from the dystrophic mice. J Neuropathol Exp Neurol 34:517–530.

Bray GM, Cullen MJ, Aguayo AJ, Rasminsky M (1979) Node-like areas of intramembranous particles in the unensheathed axons of dystrophic mice. Neurosci Lett 13:203–208.

Dugandzija-Novakovic S, Koszowski AG, Levinson SR, Shrager P (1995) Clustering of Na^+ channels and node of Ranvier formation in remyelinating axons. J Neurosci 15:492–503.

Dugandzija-Novakovic S, Deerinck TJ, Levinson SR, Shrager P, Ellisman MH (1996) Clusters of axonal Na^+ channels adjacent to remyelinating Schwann cells. J Neurocytol 25:403–412.

Ellisman MH (1976) The distribution of membrane molecular specializations characteristic of the node of Ranvier is not dependent upon myelination. Soc Neurosci Abstr 2:410.

Ellisman MH (1979) Molecular specializations of the axon membrane at nodes of Ranvier are not dependent upon myelination. J Neurocytol 8:719–735.

England JD, Gamboni F, Levinson SR (1990) Changes in the distribution of sodium channels along demyelinated axons. Proc Natl Acad Sci USA 87:6777–6780.

Engvall E, Earwicker D, Day A, Muir D, Manthorpe M, Paulsson M (1992) Merosin promotes cell attachment and neurite outgrowth and is a component of the neurite-promoting factor of the RN22 Schwannoma cells. Exp Cell Res 198:115–123.

Friede RL, Beuche W (1985) A new approach toward analyzing peripheral nerve fiber populations. I. Variance in sheath thickness corresponds to different geometric proportions of the internodes. J Neuropathol Exp Neurol 44:60–72.

Joe EH, Angelides K (1992) Clustering of voltage-dependent sodium channels on axons depends on Schwann cell contact. Nature 356:333–335.

Kaplan MR, Meyer-Franke A, Lambert S, Bennett V, Levinson SR, Barres BA (1996) A soluble oligodendrocyte-derived signal induces regularly spaced sodium channel clusters along CNS axons *in vitro*. Soc Neurosci Abstr 1:32.

Kordeli E, Davis J, Trapp B, Bennett V (1990) An isoform of ankyrin is colocalized at the nodes of Ranvier in myelinated axons of central and peripheral nerves. J Cell Biol 110:1341–1352.

Kordeli E, Lambert S, Bennett V (1995) $Ankyrin_G$: a new ankyrin gene with neural-specific isoforms localized at the axonal initial segment and node of Ranvier. J Biol Chem 270:2352–2359.

Nitkin RM, Wallace BG, Spira ME, Godfrey EW, McMahan UJ (1983) Molecular components of the synaptic basal lamina that direct differentiation of regenerating neuromuscular junctions. Cold Spring Harb Symp Quant Biol 48:653–665.

Ritchie JM, Black JA, Waxman SG, Angelides KJ (1990) Sodium channels in the cytoplasm of Schwann cells. Proc Natl Acad Sci USA 87:9290–9294.

Rosenbluth J (1988) Role of glial cells in the differentiation and function of myelinated axons. Int J Dev Neurosci 6:3–24.

Rosenbluth J, Blakemore W (1984) Structural specializations of chronically demyelinated spinal cord axons in cat as seen in freeze fracture replicas. Neurosci Lett 48:171–177.

Sharp AA, Caldwell JH (1996) Aggregation of sodium channels induced by a postnatally upregulated isoform of agrin. J Neurosci 16:6775–6783.

Smith KJ, Bostock H, Hall SM (1982) Saltatory conduction precedes remyelination in axons demyelinated with lysophosphatidyl choline. J Neurol Sci 54:13–31.

Srinivasan Y, Elmer L, Davis J, Bennett J, Angelides K (1988) Ankyrin and spectrin associate with voltage-dependent sodium channels in brain. Nature 333:177–180.

Stirling CA (1975) Abnormalities in Schwann cell sheaths in spinal nerve roots of dystrophic mice. J Anat 119:169–180.

Sunada Y, Bernier SM, Kozak CA, Yamada Y, Campbell K (1994) Deficiency of merosin in dystrophic *dy* mice and genetic linkage of laminin M chain gene to *dy* locus. J Biol Chem 269:13729–13732.

Vabnick I, Novakovic SD, Levinson SR, Schachner M, Shrager P (1996) The clustering of axonal sodium channels during development of the peripheral nervous system. J Neurosci 16:4914–4922.

Waxman SG, Black JA, Foster RE (1982) Freeze fracture heterogeneity of the axolemma of premyelinated fibers in the CNS. Neurology 32:418–421.

Wiley-Livingston CA, Ellisman MH (1980) Development of axonal membrane specializations defines nodes of Ranvier and precedes Schwann cell myelin elaboration. Dev Biol 79:334–355.

Wiley-Livingston CA, Ellisman MH (1981) Myelination-dependent axonal membrane specializations demonstrated in insufficiently myelinated nerves of the dystrophic mouse. Brain Res 224:55–67.

Wood JG, Jean DH, Whitaker JN, McLaughlin BJ, Albers RW (1977) Immunocytochemical localization of the sodium, potassium-activated ATPase in knifefish brain. J Neurocytol 6:571–581.

Xu H, Christmas P, Wu X, Wewer U, Engvall E (1994) Defective muscle basement membrane and lack of M-laminin in the dystrophic *dy*/*dy* mouse. Proc Natl Acad Sci USA 91:5572–5576.

Zhang X, Bennett V (1996) Identification of O-linked *N*-acetyl glucosamine modification of $ankyrin_G$ isoforms targeted to nodes of Ranvier. J Biol Chem 271:31391–31398.